



RH and O₃ concentration as two prerequisites for sulfate formation

Yanhua Fang^{1#} and Chunxiang Ye^{1#}, Junxia Wang¹, Yusheng Wu¹, Min Hu¹, Lin Weili², Fanfan Xu¹, Tong Zhu^{1*}

¹BIC-ESAT and SKL-ESPC, College of Environmental Sciences and Engineering, Peking University, Beijing, 100871, China

5 ²College of Life and Environmental Sciences, Minzu University of China, Beijing 100081, China

[#]These authors contributed equally to the paper.

*Correspondence to: Tong Zhu (tzhu@pku.edu.cn)

Abstract. Sulfate formation mechanisms have been discussed extensively but are still disputed. In this work, a year-long
10 particulate matter (PM_{2.5}) sampling campaign was conducted together with measurements of gaseous pollutant concentrations
and meteorological parameters in Beijing, China, from March 2012 to February 2013. The sulfur oxidation ratio (SOR), an
indicator of secondary sulfate formation, displayed a clear summer peak and winter valley, even though no obvious seasonal
variations in sulfate mass concentration were observed. A rapid rise in the SOR was found at a RH threshold of ~45% or an
O₃ concentration threshold of ~35 ppb, suggesting that RH and O₃ concentrations were two prerequisites for rapid sulfate
15 formation, which likely occurred via multiphase reactions. H₂O₂ oxidation was proposed to be the major route of sulfate
formation, since the O₃ oxidation route has previously been shown to be unimportant. The seasonal variations in sulfate
formation could be accounted for by variations in the RH and O₃ prerequisites. For example, over the year-long study, the
fastest SO₂-to-sulfate conversion occurred in summer, which was associated with the highest values of both O₃ concentration
and RH. The SOR also displayed variations with pollution levels, i.e., the SOR increased as pollution evolved in all seasons.
20 Such variations were primarily associated with a transition from the slow gas phase formation of sulfate to rapid multiphase
reactions, since RH increased as pollution evolved. In addition, the self-catalytic nature of sulfate formation (i.e., increasing
aerosol water content with simultaneous increases in sulfate mass concentrations and RH) also contributed to variations among
the pollution scenarios. Overall, our observations validated the two prerequisites for fast sulfate formation and revealed the
seasonal and pollution level variations in sulfate formation in Beijing. H₂O₂ oxidation was the major route of sulfate formation,
25 although reactions involving transition metal ions (TMIs) and NO₂ might have also competed.

1 Introduction

Beijing, the capital of China, suffers from serious air pollution due to its rapid economic growth and urbanisation (Hu et al.,
2015a). The chemical composition and sources of fine particulate matter (PM_{2.5}) in Beijing have been studied extensively (Han
30 et al., 2015; Lv et al., 2016; Zhang et al., 2013; Zheng et al., 2005). Secondary components, especially sulfate, nitrate, and



ammonium (SNA), are the main contributors to $PM_{2.5}$ (Huang et al., 2014). On the most severely polluted days, SNA account for more than half of total $PM_{2.5}$ mass concentrations and play a more important role than on clean days (Quan et al., 2014; Wang et al., 2014b; Zheng et al., 2015b).

The kinetics and mechanisms of the formation of sulfate, a major component of SNA, are complex and remain unclear (Ervens, 2015; Harris et al., 2013; Warneck, 2018). For example, two key questions concerning sulfate formation are: (1) exactly how do various parameters influence sulfate formation, and (2) how do multiple formation routes compete and contribute together to sulfate formation under ambient conditions. In general, sulfate is produced from SO_2 via gas phase oxidation reactions involving the hydroxide radical (OH) and Criegee intermediates (Gleason et al., 1987; Sarwar et al., 2014; Vereecken et al., 2012), heterogeneous reactions (mainly on dust aerosols), and multiphase transformations with O_3 , H_2O_2 , or O_2 (catalysed by transition metal ions (TMIs) (i.e., $TMIs + O_2$) and NO_2 ($NO_2 + O_2$)) as liquid phase oxidants, which occur mainly in clouds but also in aerosol droplets near the ground (Zhu et al., 2011).

Due to the major role of multiphase transformations, sulfate production is presumed to be self-catalysed, i.e., the formation of hydrophilic sulfate aerosols under high relative humidity (RH) conditions results in an increase in aerosol water content (AWC), which results in greater particle volume for further multiphase reactions (Cheng et al., 2016; Pan et al., 2009; Xu et al., 2017). Analyses of the correlation of sulfate formation with RH and AWC have been conducted to test this hypothesis, using the concept of the sulfur oxidation ratio (SOR), defined as the molar ratio of sulfate to total sulfur (= sulfate + SO_2). It is used to indicate the magnitude of the secondary formation of sulfate and expressed as (Wang et al., 2005):

$$SOR = \frac{n_{SO_4^{2-}}}{n_{SO_4^{2-}} + n_{SO_2}}, \quad (\text{Eq. 1})$$

where $n_{SO_4^{2-}}$ and n_{SO_2} represent the molar concentrations of sulfate and SO_2 , respectively.

Sun et al. (2014; 2013) found positive correlations between the SOR and RH, and observed rapid increases in SORs at elevated RH levels. Xu et al. (2017) found positive correlations of the SOR with both RH and AWC. Multiphase transformation routes, including O_3 oxidation, $TMIs + O_2$, and $NO_2 + O_2$ routes, are pH-sensitive and suppressed at low pH (Seinfeld and Pandis, 2006). Sulfate production raises the acidity of aerosols and therefore the multiphase transformations of sulfate are presumed to be self-constrained (Cheng et al., 2016). For example, a significant contribution from the O_3 oxidation route can only be expected under alkaline conditions (e.g., sea-salt), otherwise, O_3 oxidation is only a minor pathway for sulfate formation (Alexander et al., 2005; Sievering et al., 2004). How the self-constraining nature of sulfate formation influences the relative significance of the $TMI + O_2$ and $NO_2 + O_2$ routes is still under debate. Cheng et al. (2016) proposed that the $NO_2 + O_2$ route is important during severe haze under neutral conditions (He et al., 2018; Wang et al., 2016). Guo et al. (2017) suggested that aerosols are acidic in Beijing (except for during the limited cases of dust or sea-salt events), casting doubt on the importance of the $NO_2 + O_2$ route in sulfate formation (Liu et al., 2017a). According to laboratory-based Raman spectroscopy studies, sulfate can be produced via the aqueous oxidation of SO_2 by $NO_2 + O_2$, with an SO_2 reactive uptake coefficient of 10^{-5} , which represents an atmospherically relevant value (Yu et al., 2018), whereas others have suggested that this route is of minor importance in the atmosphere (Li et al., 2018; Zhao et al., 2018). In addition, Xie et al. (2015) proposed that NO_2 could enhance



the formation of sulfate in certain cases, for example, in biomass burning plumes or dust storms (He et al., 2014). Evaluation of the contribution of TMI + O₂ reactions appears to be more complex since it depends on aerosol acidity, solubility, oxidation state, and the synergistic effects of different TMIs (Deguillaume et al., 2005; Warneck, 2018).

The compensating effects among AWC, aerosol acidity, and the concentrations of precursors and catalysts show that the kinetics and mechanisms of sulfate formation are highly complex. It can be inferred that there is competition between the various routes, with dependences on atmospheric conditions (e.g., seasonal and pollution level variations) likely, but this has not received much research attention previously. Here, daily PM_{2.5} samples were collected in Beijing from March 2012 to February 2013 and their chemical composition was analysed. The main parameters that influenced sulfate formation (i.e., RH, O₃ concentration, TMIs, etc.) were determined. This valuable dataset enabled us to explore: (1) the specific role of each influencing factor in sulfate formation, and (2) how multiple sulfate formation routes compete in different seasons and under various pollution scenarios.

2 Measurements and methodology

2.1 Measurements

2.1.1 Measurement stations

The two measurement stations are shown in Figure 1. The PKU station (116.30 °E, 39.99 °N) is about 20 m above ground level on the campus of Peking University, Beijing, China (Liang et al., 2017). Daily PM_{2.5} samples were collected using a four-channel sampler (TH-16A; Wuhan Tianhong Instruments, China) at a flow rate of 16.7 L min⁻¹ from 1 March 2012 to 28 February 2013. The gaseous pollutants SO₂, NO_x, and O₃ were measured with a pulsed fluorescence SO₂ analyser (Model 43i TLE; Thermo Fisher Scientific, Waltham, MA, USA), chemiluminescence NO–NO₂–NO_x analyser (Model 42i TL; Thermo Fisher Scientific), and an ultraviolet photometric O₃ analyser (Model 49i; Thermo Fisher Scientific), respectively. Temperature and RH were also monitored (MSO; Met One Instruments, Grants Pass, OR, USA). Solar radiation data were obtained from the Beijing Meteorological Observatory Station.

2.1.2 Filter sampling and analysis

Each PM_{2.5} sample set consisted of one quartz filter (47 mm; Whatman QM/A, Maidstone, England) and three Teflon filters (47 mm; pore size = 2 μm; Whatman PTFE). The quartz filters were baked for 5.5 h at 550 °C before use. The Teflon filters were weighed in a weighing room before and after sampling using a delta range balance (0.01 mg/0.1 mg precision; AX105; Mettler Toledo, Switzerland). To minimise contamination, all Teflon filters were placed in a super clean room (temperature = 22 ± 1 °C; RH = 40 ± 2%) for 24 h before being weighed. After sampling, all filters were stored at –20 °C prior to analysis.

Water soluble cations (Na⁺, NH₄⁺, K⁺, Mg²⁺, and Ca²⁺) and anions (SO₄²⁻, NO₃⁻, Cl⁻, and F⁻) were measured using ion chromatography (ICS-2500 and ICS-2000; DIONEX, USA). Trace elements (Na, Mg, Al, Ca, Ti, Cr, Mn, Fe, Co, Ni, Cu, Zn,



Se, Mo, Cd, Ba, Tl, Pb, Th, and U) were analysed by inductively coupled plasma–mass spectrometry (ICP–MS, X-Series; Thermo Fisher Scientific). Organic carbon (OC) and elemental carbon (EC) were measured using a thermal/optical carbon analyser (RT-4; Sunset Laboratory Inc., Tigard, OR, USA). The procedure for the measurement of water soluble Fe has been described in detail in a previous study (Xu et al., 2018).

5 2.2 Estimation of the mass concentrations of PM_{2.5} components

The chemical components of PM_{2.5} were divided into seven categories according to their source type: sulfate, nitrate, ammonium, organic matter (OM), EC, minerals, and trace element oxides (TEOs). The mass concentrations of OM, minerals, and TEOs were calculated from OC, Al, and trace element concentrations, respectively. The details of this method are provided in the supplementary information (SI). For minerals, validation of the method using only Al to represent all minerals is shown in Fig. S2. TEOs mostly originated from anthropogenic sources (Fig. S3).

2.3 Quality assurance and quality control

The PM_{2.5} sampling instruments were cleaned and calibrated every 2–3 months. Before the daily filter replacement, filter plates were scrubbed with degreasing cotton that had been immersed in dichloromethane. For water-soluble ions, OC/EC, and trace element measurements, standard solutions were analysed before each series of measurements. The R^2 values of the calibration curves were all > 0.999. For water-soluble ion measurements, beakers, tweezers, and vials were cleaned with deionised water (18.2 MΩ; Milli-Q, USA) three times before use. Certified reference standards (National Institute of Metrology, China) were used for calibration. For OC/EC measurements, tweezers and scissors were scrubbed with degreasing cotton immersed in dichloromethane for every filter. Total organic carbon (TOC) was calculated based on calibration with external standard solutions. For trace element measurements, containers and tweezers were cleaned three times with nitric acid before use, and the analysis of a certified reference standard (NIST SRM-2783) was used to verify accuracy. The recovery of all measured trace elements fell within ±20% of their certified values. For gaseous pollutants and meteorological parameters, all instruments were maintained and calibrated weekly based on manufacturers' protocols.

3 Results and discussion

3.1 General description

The annual and seasonal mean (± one standard deviation (SD)) concentrations of PM_{2.5} and its seven major components are summarised in Table 1. The annual mean PM_{2.5} concentration was 84.1 (±63.1) μg m⁻³, which is more than two times greater than the Chinese National Ambient Air Standard of 35 μg m⁻³. On 145 of the 318 (46%) measurement days, daily mean PM_{2.5} concentrations were above the Chinese National Ambient Air Standard 24 h mean concentration of 75 μg m⁻³. Time series of PM_{2.5} concentrations and its seven major components are shown in Fig. 2. Seasonal variations in PM_{2.5} loading are obvious, with spring and winter peaks and summer and autumn valleys. OM and EC concentrations display common seasonal variations,



with a plateau from mid-October to mid-February and a valley in summer (Fig. 2), which resembles the variations in $PM_{2.5}$, K^+ , and Cl^- (Figs. 2 and 4). Further investigation revealed that primary organic matter (POM) was the main component of OM (Fig. S4). These results suggest that OM, EC, K^+ , and Cl^- may have originated from a common primary source. There are clear temperature dependencies among OM, EC, K^+ , and Cl^- concentrations, which are elevated at low temperatures (i.e., -5 to 15 °C) (Fig. S5). Coal combustion for heating purposes was initially considered to be their common source. However, a tracer of coal combustion emissions, Se (Ranville et al., 2010), exhibits different seasonal variations, with a concentration valley from spring to mid-October (Fig. 4). The Se concentrations had a strong dependence on temperature, where high concentrations appeared only when the temperature was below 0 °C (Fig. S5). The period with high Se concentrations coincided with the heating season in Beijing in 2013 (Fig. 4). Therefore, we further conclude that OM, EC, K^+ , and Cl^- did originate from anthropogenic sources, but that coal combustion was not their sole primary source. Other anthropogenic sources should be considered, such as biomass burning, to account for the emissions of OM, EC, K^+ , and Cl^- during the heating season (Liang et al., 2017; Tan et al., 2016; Zhang et al., 2015b). Overall, anthropogenic sources contributed much more to $PM_{2.5}$ mass loading from mid-October to mid-February than in summer and early autumn. Changes in anthropogenic sources thus dominated the seasonal variations in $PM_{2.5}$ and might have implications for secondary chemistry, such as sulfate formation. SNA accounted for more than one-third of $PM_{2.5}$ annually and showed similar seasonal variations to that of $PM_{2.5}$ (Fig. 2), with the notable exception that sulfate became the highest contributor to $PM_{2.5}$ (~25%) in summer (Fig. 3). The summer peak in sulfate could be accounted for by fast secondary formation, as will be discussed later.

The seasonal variations in minerals also indicated an important contribution of dust events to $PM_{2.5}$ loading during spring, which is a well-known phenomenon (Zhang et al., 2003; Zhuang et al., 2001). TEOs display no obvious seasonal variations (Fig. 2). Based on the high enrichment factors of most TEOs, they were mostly derived from anthropogenic sources (Fig. S3). For example, the sources of Zn and Pb include industrial combustion and waste incineration (Hu et al., 2015b). There was no clear explanation for the lack of seasonal variations in TEOs.

On an annual basis, the seven major components accounted for over 80% of $PM_{2.5}$ (Fig. 3). The diversity of the seasonal variations in $PM_{2.5}$ and its major components found in our study imply that there were seasonal variations in both the primary sources and secondary formation of $PM_{2.5}$.

3.2 Influence of various parameters on sulfate formation

To further explore the parameters that influenced sulfate formation, SORs were plotted against RH and the concentrations of O_3 , NO_2 , and Fe (total Fe, including both water soluble and water insoluble Fe), which is a major tracer of transition metals (Figs. 5 and 6).

As shown in Fig. 5a, an RH threshold of ~45% was critical for efficient SO_2 oxidation (i.e., a high SOR). Such a threshold effect was thought to be reasonable given that aerosol water content (AWC) increases sharply at a given RH threshold, at which the aerosol undergoes a phase transition from a (semi-)solid particle to a droplet (Pan et al., 2009; Russell and Ming,



2002). Our observation of a daily average RH threshold of ~45% is in line with previous reports of 40–50% (Liu et al., 2015; Quan et al., 2015; Xu et al., 2017; Yang et al., 2015; Zheng et al., 2015b), but is slightly lower than the *in situ* phase transition threshold RH of 50–60% previously observed in Beijing (Liu et al., 2017b). Correlation analysis of SOR and RH (or AWC) has often been conducted in previous studies. For example, Wang et al. (2005) found a weak positive correlation of SORs with
5 RH ($R = 0.38$), while Sun et al. (2006) found a strong positive correlation ($R = 0.96$). However, the analysis in the present work and those of a few previous studies revealed that the relationship between the SOR and RH is nonlinear (Sun et al., 2013; Sun et al., 2014; Zheng et al., 2015b). In fact, the RH threshold suggests that high RH (or AWC) is a prerequisite for fast sulfate formation via multiphase reactions, which are known to account for the majority of sulfate accumulation.

From the large scattering of data points around the fit line in Fig. 5a, it might be inferred that RH was not the only prerequisite
10 for fast SO₂-to-sulfate conversion. As shown in Fig. 5b, a significant increase in the SOR was also observed at an O₃ concentration threshold of ~35 ppb. High O₃ concentrations (i.e., > 35 ppb) were accompanied by high SOR values of ~0.4 (right-hand side of Fig. 5b). Correlation analyses of SORs with O₃ have been conducted but inconsistent results were reported. Wang et al. (2005) found a weak positive correlation between SORs and O₃ ($R = 0.47$) for continuous observations in Beijing during 2001–2003. However, Liu et al (2015) found a weak negative correlation between SORs and O₃ ($R = -0.53$, $p = 0.01$)
15 during a haze episode in September 2011. Zhang et al. (2018) found no correlation between SORs and O₃ during winter haze days in 2015. Quan et al. (2015) found that the SOR decreased with O₃ when O₃ concentrations were lower than 15 ppb, but increased with O₃ when O₃ concentrations were higher than 15 ppb, for observations made during autumn and winter 2012. In the present study, our observations revealed that the relationship between the SOR and O₃ concentration, like RH, was nonlinear and that a high O₃ concentration was another prerequisite for fast sulfate formation. Such a conclusion was a surprise
20 first, since O₃ oxidation was not thought to be a major route for SO₂-to-sulfate conversion (Sievering et al., 2004). However, as a primary precursor to OH radicals and H₂O₂ (via HO₂), O₃ is also considered to be a proxy for atmospheric oxidative capacity (Lelieveld et al., 2016; Lu et al., 2017). High O₃ concentrations (e.g., > 35 ppb) correspond to a strong oxidative capacity, which favors multiphase sulfate formation and thus a high SOR, whereas low O₃ concentrations suggest a lack of available oxidants for multiphase SO₂-to-sulfate conversion and thus a low SOR. In addition, the simultaneous occurrence of
25 low SORs and low O₃ concentrations had a secondary cause. Low O₃ concentrations in the Beijing urban area were often due to the titration of O₃ by NO (Li et al., 2016), which accumulated together with SO₂ (Fig. S6). The accumulation of SO₂, which “diluted” the SOR (Eq. 1), was thus naturally accompanied by the titration of O₃. The L-shaped dependence of the SOR on several other primary pollutants, such as EC, NO, and Se (Fig. S7), further confirmed this secondary cause. Therefore, the accumulation of primary pollutants might also help to explain the low SOR values of ~0.1 on the left-hand side of Fig. 5b, in
30 addition to the lack of available oxidants for multiphase SO₂-to-sulfate conversion.

The large scattering of data points around the fit line in Fig. 5b suggests that O₃ concentration, like RH, was not the only prerequisite for fast SO₂-to-sulfate conversion. The dependence of the SOR on RH was separated into low (< 35 ppb) and high (> 35 ppb) O₃ groups (solid black circles and solid blue circles, respectively, in Fig. 5a). SOR values above the fit line are found mostly for the high O₃ group. After the dependency of the SOR on O₃ concentration was separated into low (< 45%)



and high (> 45%) RH groups (solid black circles and solid blue circles, respectively, in Fig. 5b), a similar pattern was found for the high RH group. In other words, fast multiphase SO₂-to-sulfate conversion could only occur when both O₃ and RH exceeded their respective thresholds simultaneously. As the O₃ oxidation route can be excluded in a heavily polluted area with high aerosol acidity (Shen et al., 2012; Sievering et al., 2004), such as Beijing, the two prerequisites suggest that H₂O₂ oxidation might be the major sulfate formation route. Such a conclusion is supported by a recent report of model underestimations of H₂O₂ concentrations in the Beijing area (Ye et al., 2018).

No clear dependence of the SOR on concentrations of Fe or NO₂ was found (Figs. 6a and 6b). Possible reasons and implications of this result will be discussed in the following section. There is currently no available direct measurement for aerosol pH (Rindelaub et al., 2016), and it is not possible to perform a proxy calculation for estimation of aerosol acidity from the data collected in this work, hence discussion of the self-constrained nature of sulfate formation is beyond the scope of our study.

3.3 Implications for sulfate formation mechanisms

Our observations of the factors that influence sulfate formation have implications for sulfate formation routes and the variations among mechanisms. Thresholds in RH and O₃ concentrations were found to be critical to the SOR, suggesting that AWC and atmospheric oxidative capacity were two prerequisites for fast multiphase SO₂-to-sulfate conversion. These dependences imply that H₂O₂ oxidation played a major role in sulfate formation, as the O₃ oxidation route could be excluded due to the strong aerosol acidity in environments such as Beijing, as was stated above. The plot of SORs against Fe, the dominant transition metal species, shows no clear dependence (Figs. 6a and S8). However, such a pattern did not exclude TMIs + O₂ as a major route for sulfate formation. Possible explanations for the lack of an Fe dependence are: (1) Fe was accompanied by low RH and O₃ concentrations, which are the two main prerequisites for fast SO₂-to-sulfate conversion, and (2) Fe acted as a catalyst and thus its concentration might not be directly proportional to that of the reaction product, sulfate. The relationships of Fe with RH and O₃ were examined and the results suggest that TMIs were not related to RH or O₃ concentrations (Figs. 6c and 6d), which excluded the first possibility. The plot of SORs against NO₂ shows no clear dependence either (Fig. 6b). However, such a pattern does not exclude NO₂-based reactions as major routes of sulfate formation. Several laboratory studies excluded NO₂ as a direct oxidant in SO₂-to-sulfate conversion. For example, Zhao et al. (2018) tested the oxidation of SO₂ by NO₂ in an N₂ atmosphere and concluded that NO₂ is not an important oxidant, since NO₂ was more likely to undergo disproportionation (Li et al., 2018). However, Yu et al. (2018) further explored this reaction, and found that the reaction rate was 2–3 orders of magnitude greater in an O₂ + N₂ atmosphere, indicating potentially important roles of NO₂ + O₂ oxidation in sulfate formation (He et al., 2014; Ma et al., 2018). As with Fe, if NO₂ acted as a catalyst, its concentration might not be directly proportional to that of sulfate. Previously, aerosol surface area and concentrations of Fe, Mn, and NO₂ were used in model evaluations of catalytic sulfate formation in the boundary layer (Wang et al., 2014a; Zheng et al., 2015a). However, our observations suggest that a careful reassessment of such calculations is required. In addition, model calculations have often suggested important contributions of in-cloud processes to sulfate accumulation near the ground (Barth et al., 2000), although few observational constraints are available for confirmation of these model results (Harris et al., 2014; Shen et al., 2012). The O₃ concentration



and RH prerequisites found in the present work might indicate a major role of *in situ* sulfate formation in the boundary layer, via multiphase reactions with H_2O_2 as the main oxidant, rather than in-cloud processes and intrusion from the free troposphere. As the two prerequisites showed strong seasonal and pollution level variations over the measurement year, the SOR exhibited corresponding variations. As shown in Fig. 7, SORs display clear seasonal variations, with the highest value (± 1 SD) of 0.46
5 (± 0.22) in summer, followed by spring (0.23 ± 0.14), autumn (0.18 ± 0.15), and winter (0.09 ± 0.05). The highest SOR (i.e., fastest SO_2 -to-sulfate conversion rate) was found in summer, which is not surprising because the ambient conditions in summer were conducive SO_2 -to-sulfate conversion (Wang et al., 2005). RH and O_3 concentrations in summer were not only the highest in the year, but on average were also both higher than their thresholds of 45% and 35 ppb, respectively, which was unique among the four seasons. In summer, the median and mean (± 1 SD) RH levels were 57.4% and 57.6 (± 13.6)%, respectively,
10 and the median and mean O_3 concentrations were 46.9 ppb and 46.0 (± 18.3) ppb. It should be noted that the median and mean SO_2 concentrations were 2.6 and 4.0 (± 3.7) ppb, respectively, which were the lowest in the year. Despite the low concentrations of SO_2 , there were considerable sulfate concentrations (Figs. 2 and 7), which can be accounted for by fast SO_2 -to-sulfate conversion. As discussed above, H_2O_2 oxidation could have been a major route of sulfate formation. Direct measurements of aqueous H_2O_2 were not conducted in this study, but the H_2O_2 concentrations in Beijing reported by Fu (2014) were found to
15 be highest in summer and elevated from March to November 2013. Although the rapid accumulation of secondary sulfate during winter haze days in Beijing has been widely reported (Wang et al., 2014b; Zheng et al., 2015b), the lowest SOR was observed during winter in the present study (Fig. 7a), which is consistent with previous observations (Wang et al., 2005). On winter haze days, RH values of up to 73.6% and $\text{PM}_{2.5}$ mass loadings of up to $375.3 \mu\text{g m}^{-3}$ were observed. Therefore, AWC was not the limiting factor in SO_2 -to-sulfate conversion (Figs. 7b and 7e). The SO_2 -to-sulfate conversion rate in winter could
20 have been limited by the reduced atmospheric oxidative capacity (Fig. 7c), which was a result of both high emissions of the primary pollutant NO (Fig. S9) and low solar radiation levels (Fig. 7f). Sulfate concentrations in winter were comparable to those in summer, which might have been driven by high SO_2 concentrations in winter (Fig. 7d), despite slow SO_2 -to-sulfate conversion. The lower boundary layer height in winter relative to other seasons would also have encouraged the accumulation of both $\text{PM}_{2.5}$ and its components, including sulfate (Gao et al., 2015; Zhang et al., 2015a). The SORs in spring and autumn
25 were comparable and moderate, possibly representing a transition in conditions between summer and winter. For each season, four pollution scenarios were classified according to $\text{PM}_{2.5}$ level. The lowest 25%, 25–50%, 50–75%, and highest 25% of pollution levels were defined as “clean”, “formation”, “evolution”, and “further evolution”, respectively. The relative contributions of seven major components of $\text{PM}_{2.5}$ among the four pollution scenarios are shown in Fig. 8. In all four seasons, the relative contribution of SNA increased with $\text{PM}_{2.5}$ loading. This phenomenon has been reported in previous studies,
30 but data availability was limited in autumn (Xu et al., 2017) and winter (Zheng et al., 2015b). The SOR increased consistently in all four seasons as pollution accumulated, where both the highest value and strongest variability were observed in summer (Fig. 9a). Although SO_2 should have reduced the SOR (Eq. 1), concurrent increases in primary SO_2 and SORs were observed (Figs. 9a and 9b), indicating a significant increase in the SO_2 -to-sulfate conversion rate with $\text{PM}_{2.5}$ loading, which offset the “dilution” effect (Eq. 1). Such variations in sulfate formation with pollution levels can be accounted for by the corresponding



variations in both O₃ concentrations and RH (Figs. 9c and 9d). In all four seasons, RH increased consistently as pollution accumulated (Fig. 9d). O₃ concentrations decreased consistently as pollution evolved in all of the seasons except for summer (Fig. 9c). The increase in SO₂-to-sulfate conversion with PM_{2.5} loading can be attributed to the self-catalytic nature of the multiphase formation of sulfate, i.e., both RH and PM_{2.5} increased continuously with the accumulation of PM_{2.5}, resulting in a rapid rise in AWC and providing greater reaction volume for further sulfate formation. Therefore, the increases in RH and PM_{2.5} could have compensated for the weak oxidative capacity, resulting in fast sulfate formation as pollution evolved. Particularly in summer, not only did both RH and O₃ concentrations increase as pollution evolved, but both RH and O₃ concentrations were generally above their respective thresholds at all pollution levels (dashed lines in Figs. 9c and 9d). This explains our observations of both the highest value and strongest dependence on pollution level for SORs in summer.

4 Conclusions

In this study, the annual mean concentration of PM_{2.5} in Beijing during 2012–2013 was 84.1 (± 63.1) μg m⁻³, with clear seasonal and pollution level variations in its chemical components, highlighting the contribution of SNA formation to the accumulation of PM_{2.5} in all seasons. RH and O₃ concentrations were identified as two prerequisites for fast SO₂-to-sulfate conversion. RH above a threshold of ~45% greatly accelerated the conversion rate. A similar effect was also found for O₃ at a concentration threshold of ~35 ppb. Such dependences have interesting implications. First, they indicate a major role of the H₂O₂ route in sulfate formation, which might further indicate a major role of *in situ* sulfate production in the boundary layer, rather than in-cloud processes and intrusion from the free troposphere. Second, the observed dependences were also able to account for the seasonal and pollution level variations in SO₂-to-sulfate conversion rates. Both the highest value and strongest variability of SOR were observed in summer, which might be attributed to the highest values of O₃ concentrations and RH in summer. SO₂-to-sulfate conversion accelerated as pollution accumulated, which was primarily attributed to a shift from gas phase oxidation to the multiphase oxidation route, which is self-catalytic in nature. The increase in RH was able to offset the low oxidative capacity under heavily polluted conditions, and resulted in increasingly fast SO₂-to-sulfate conversion as pollution accumulated. While our simultaneous observations of the SOR and concentrations of Fe and NO₂ could not exclude TMI + O₂ and NO₂-based reactions, a reassessment of the relationships between sulfate formation, aerosol surface area and the concentrations of Fe and NO₂ is necessary.

Author contributions

TZ designed the study. YHF, CXY, and TZ prepared the manuscript with input from all co-authors. YHF and JXW collected and weighed the PM_{2.5} filter samples and carried out the analysis of the components of PM_{2.5}. FFX carried out the measurement of water soluble Fe. YSW and MH provided the data for gaseous pollutants, temperature, and RH. WLL provided the solar radiation data.



Competing interests.

The authors declare that they have no conflict of interest.

Acknowledgements

This work was supported by the National Natural Science Foundation Committee of China (91544000, 41121004, and
5 91744206). We also thank Dr. Robert Woodward-Massey for his kind help in English writing.

References

- Alexander, B., Park, R. J., Jacob, D. J., Li, Q. B., Yantosca, R. M., Savarino, J., Lee, C. C. W., and Thiemens, M. H.: Sulfate formation in sea-salt aerosols: Constraints from oxygen isotopes, *J. Geophys. Res.*, 110, <https://doi.org/10.1029/2004JD005659>, 2005.
- 10 Barth, M. C., Rasch, P. J., Kiehl, J. T., Benkovitz, C. M., and Schwartz, S. E.: Sulfur chemistry in the National Center for Atmospheric Research Community Climate Model: Description, evaluation, features, and sensitivity to aqueous chemistry, *J. Geophys. Res. Atmos.*, 105, 1387-1415, <https://doi.org/10.1029/1999jd900773>, 2000.
- Cheng, Y. F., Zheng, G. J., Wei, C., Mu, Q., Zheng, B., Wang, Z. B., Gao, M., Zhang, Q., He, K. B., Carmichael, G., Poschl, U., and Su, H.: Reactive nitrogen chemistry in aerosol water as a source of sulfate during haze events in China, *Science Advances*, 2, <https://doi.org/10.1126/sciadv.1601530>, 2016.
- 15 Deguillaume, L., Leriche, M., Desboeufs, K., Mailhot, G., George, C., and Chaumerliac, N.: Transition metals in atmospheric liquid phases: Sources, reactivity, and sensitive parameters, *Chem. Rev.*, 105, 3388-3431, <https://doi.org/10.1002/chin.200549218>, 2005.
- Ervens, B.: Modeling the processing of aerosol and trace gases in clouds and fogs, *Chem. Rev.*, 115, <https://doi.org/10.1021/cr5005887>, 2015.
- 20 Fu, A. Y.: Study on peroxide concentration and its influence factors in the urban atmosphere, Master, Zhengjiang University, 2014.
- Gao, Y., Zhang, M., Liu, Z., Wang, L., Wang, P., Xia, X., Tao, M., and Zhu, L.: Modeling the feedback between aerosol and meteorological variables in the atmospheric boundary layer during a severe fog-haze event over the North China Plain, *Atmos. Chem. Phys.*, 15, 4279-4295, <https://doi.org/10.5194/acp-15-4279-2015>, 2015.
- 25 Gleason, J. F., Sinha, A., and Howard, C. J.: Kinetics of the gas phase reaction $\text{HOSO}_2 + \text{O}_2 \rightarrow \text{HO}_2 + \text{SO}_3$, *J. Phys. Chem.*, 91, 719-724, <https://doi.org/10.1021/j100287a045>, 1987.
- Guo, H., Weber, R. J., and Nenes, A.: High levels of ammonia do not raise fine particle pH sufficiently to yield nitrogen oxide-dominated sulfate production, *Sci. Rep.*, 7, 12109, <https://doi.org/10.1038/s41598-017-11704-0>, 2017.
- 30 Han, L., Cheng, S., Zhuang, G., Ning, H., Wang, H., Wei, W., and Zhao, X.: The changes and long-range transport of $\text{PM}_{2.5}$ in Beijing in the past decade, *Atmos. Environ.*, 110, 186-195, <http://dx.doi.org/10.1016/j.atmosenv.2015.03.013>, 2015.



- Harris, E., Sinha, B., van Pinxteren, D., Tilgner, A., Fomba, K. W., Schneider, J., Roth, A., Gnauk, T., Fahlbusch, B., Mertes, S., Lee, T., Collett, J., Foley, S., Borrmann, S., Hoppe, P., and Herrmann, H.: Enhanced role of transition metal ion catalysis during in-cloud oxidation of SO₂, *Science*, 340, 727-730, <https://doi.org/10.1126/science.1230911>, 2013.
- Harris, E., Sinha, B., van Pinxteren, D., Schneider, J., Poulain, L., Collett, J., D'Anna, B., Fahlbusch, B., Foley, S., Fomba, K. W., George, C., Gnauk, T., Henning, S., Lee, T., Mertes, S., Roth, A., Stratmann, F., Borrmann, S., Hoppe, P., and Herrmann, H.: In-cloud sulfate addition to single particles resolved with sulfur isotope analysis during HCCT-2010, *Atmos. Chem. Phys.*, 14, 4219-4235, <https://doi.org/10.5194/acp-14-4219-2014>, 2014.
- He, H., Wang, Y., Ma, Q., Ma, J., Chu, B., Ji, D., Tang, G., Liu, C., Zhang, H., and Hao, J.: Mineral dust and NO_x promote the conversion of SO₂ to sulfate in heavy pollution days, *Sci. Rep.*, 4, <https://doi.org/10.1038/srep04172>, 2014.
- He, P., Alexander, B., Geng, L., Chi, X., Fan, S., Zhan, H., Kang, H., Zheng, G., Cheng, Y., Su, H., Liu, C., and Xie, Z.: Isotopic constraints on heterogeneous sulfate production in Beijing haze, *Atmos. Chem. Phys.*, 18, 5515-5528, <https://doi.org/10.5194/acp-18-5515-2018>, 2018.
- Hu, M., Guo, S., Peng, J.-f., and Wu, Z.-j.: Insight into characteristics and sources of PM_{2.5} in the Beijing-Tianjin-Hebei region, China, *Nati. Sci. Rew.*, 2, 257-258, <https://doi.org/10.1093/nsr/nwv003>, 2015a.
- Hu, Y., Lin, J., Zhang, S., Kong, L., Fu, H., and Chen, J.: Identification of the typical metal particles among haze, fog, and clear episodes in the Beijing atmosphere, *Sci. Total. Environ.*, 511, 369-380, <http://dx.doi.org/10.1016/j.scitotenv.2014.12.071>, 2015b.
- Huang, R. J., Zhang, Y. L., Bozzetti, C., Ho, K. F., Cao, J. J., Han, Y. M., Daellenbach, K. R., Slowik, J. G., Platt, S. M., Canonaco, F., Zotter, P., Wolf, R., Pieber, S. M., Bruns, E. A., Crippa, M., Ciarelli, G., Piazzalunga, A., Schwikowski, M., Abbazade, G., Schnelle-Kreis, J., Zimmermann, R., An, Z. S., Szidat, S., Baltensperger, U., El Haddad, I., and Prevot, A. S. H.: High secondary aerosol contribution to particulate pollution during haze events in China, *Nature*, 514, 218-222, <https://doi.org/10.1038/nature13774>, 2014.
- Lelieveld, J., Gromov, S., Pozzer, A., and Taraborrelli, D.: Global tropospheric hydroxyl distribution, budget and reactivity, *Atmos. Chem. Phys.*, 16, 12477-12493, <https://doi.org/10.5194/acp-16-12477-2016>, 2016.
- Li, L., Hoffmann, M. R., and Colussi, A. J.: The role of nitrogen dioxide in the production of sulfate during Chinese haze-aerosol episodes, *Environ. Sci. Technol.*, 52, <https://doi.org/10.1021/acs.est.7b05222>, 2018.
- Li, Y. R., Ye, C. X., Liu, J., Zhu, Y., Wang, J. X., Tan, Z. Q., Lin, W. L., Zeng, L. M., and Zhu, T.: Observation of regional air pollutant transport between the megacity Beijing and the North China Plain, *Atmos. Chem. Phys.*, 16, 14265-14283, <https://doi.org/10.5194/acp-16-14265-2016>, 2016.
- Liang, P., Zhu, T., Fang, Y., Li, Y., Han, Y., Wu, Y., Hu, M., and Wang, J.: The role of meteorological conditions and pollution control strategies in reducing air pollution in Beijing during APEC 2014 and Victory Parade 2015, *Atmos. Chem. Phys.*, 17, 13921-13940, <https://doi.org/10.5194/acp-17-13921-2017>, 2017.
- Liu, M., Song, Y., Zhou, T., Xu, Z., Yan, C., Zheng, M., Wu, Z., Hu, M., Wu, Y., and Zhu, T.: Fine particle pH during severe haze episodes in northern China, *Geophys. Res. Lett.*, 44, 5213-5221, <https://doi.org/10.1002/2017GL073210>, 2017a.



- Liu, X., Sun, K., Qu, Y., Hu, M., Sun, Y., Zhang, F., and Zhang, Y.: Secondary formation of sulfate and nitrate during a haze episode in megacity Beijing, China, *Aerosol Air Qual. Res.*, 2246-2257, <https://doi.org/10.4209/aaqr.2014.12.0321>, 2015.
- Liu, Y. C., Wu, Z. J., Wang, Y., Xiao, Y., Gu, F. T., Zheng, J., Tan, T. Y., Shang, D. J., Wu, Y. S., Zeng, L. M., Hu, M., Bateman, A. P., and Martin, S. T.: Submicrometer particles are in the liquid state during heavy haze episodes in the urban atmosphere of Beijing, China, *Environ. Sci. Technol. Lett.*, 4, 427-432, <https://doi.org/10.1021/acs.estlett.7b00352>, 2017b.
- Lu, X., Chen, N., Wang, Y., Cao, W., Zhu, B., Yao, T., Fung, J. C. H., and Lau, A. K. H.: Radical budget and ozone chemistry during autumn in the atmosphere of an urban site in central China: RO_x budgets and O₃ in central China, *J. Geophys. Res. Atmos.*, 122, 3672-3685, <https://doi.org/10.1002/2016JD025676>, 2017.
- Lv, B., Zhang, B., and Bai, Y.: A systematic analysis of PM_{2.5} in Beijing and its sources from 2000 to 2012, *Atmos. Environ.*, 124, 98-108, <http://dx.doi.org/10.1016/j.atmosenv.2015.09.031>, 2016.
- Ma, J., Chu, B., Liu, J., Liu, Y., Zhang, H., and He, H.: NO_x promotion of SO₂ conversion to sulfate: An important mechanism for the occurrence of heavy haze during winter in Beijing, *Environ. Pollut.*, 233, 662, <https://doi.org/10.1016/j.envpol.2017.10.103>, 2018.
- Pan, X. L., Yan, P., Tang, J., Ma, J. Z., Wang, Z. F., Gbaguidi, A., and Sun, Y. L.: Observational study of influence of aerosol hygroscopic growth on scattering coefficient over rural area near Beijing mega-city, *Atmos. Chem. Phys.*, 9, 7519-7530, <https://doi.org/10.5194/acp-9-7519-2009>, 2009.
- Quan, J., Liu, Q., Li, X., Gao, Y., Jia, X., Sheng, J., and Liu, Y.: Effect of heterogeneous aqueous reactions on the secondary formation of inorganic aerosols during haze events, *Atmos. Environ.*, 122, 306-312, <http://dx.doi.org/10.1016/j.atmosenv.2015.09.068>, 2015.
- Quan, J. N., Tie, X. X., Zhang, Q., Liu, Q., Li, X., Gao, Y., and Zhao, D. L.: Characteristics of heavy aerosol pollution during the 2012-2013 winter in Beijing, China, *Atmos. Environ.*, 88, 83-89, <http://dx.doi.org/10.1016/j.atmosenv.2014.01.058>, 2014.
- Ranville, M. A., Cutter, G. A., Buck, C. S., Landing, W. M., Cutter, L. S., Resing, J. A., and Flegal, A. R.: Aeolian acontamination of Se and Ag in the north Pacific from Asian fossil fuel combustion, *Environ. Sci. Technol.*, 44, 1587-1593, <https://doi.org/10.1021/es902523m>, 2010.
- Rindelaub, J. D., Craig, R. L., Nandy, L., Bondy, A. L., Dutcher, C. S., Shepson, P. B., and Ault, A. P.: Direct measurement of pH in individual particles via Raman Microspectroscopy and variation in acidity with relative humidity, *J. Phys. Chem. A*, 120, <https://doi.org/10.1021/acs.jpca.5b12699>, 2016.
- Russell, L. M., and Ming, Y.: Deliquescence of small particles, *J. Chem. Phys.*, 116, 311, <https://doi.org/10.1063/1.1420727>, 2002.
- Sarwar, G., Simon, H., Fahey, K., Mathur, R., Goliff, W. S., and Stockwell, W. R.: Impact of sulfur dioxide oxidation by Stabilized Criegee Intermediate on sulfate, *Atmos. Environ.*, 85, 204-214, <http://dx.doi.org/10.1016/j.atmosenv.2013.12.013>, 2014.
- Seinfeld, J. H., and Pandis, S. N.: Atmospheric chemistry and physics: From air pollution to climate change, Second ed., John Wiley & Sons, New Jersey, 2006.



- Shen, X. H., Lee, T. Y., Guo, J., Wang, X. F., Li, P. H., Xu, P. J., Wang, Y., Ren, Y., Wang, W., Wang, T., Li, Y., Cam, S. A., and Collett, J. L.: Aqueous phase sulfate production in clouds in eastern China, *Atmos. Environ.*, 62, 502-511, <http://dx.doi.org/10.1016/j.atmosenv.2012.07.079>, 2012.
- Sievering, H., Caine, J., Harvey, M., McGregor, J., Nichol, S., and Quinn, P.: Aerosol non-sea-salt sulfate in the remote marine boundary layer under clear-sky and normal cloudiness conditions: Ocean-derived biogenic alkalinity enhances sea-salt sulfate production by ozone oxidation, *J. Geophys. Res. Atmos.*, 109, <https://doi.org/10.1029/2003jd004315>, 2004.
- Sun, Y., Wang, Z., Fu, P., Jiang, Q., Yang, T., Li, J., and Ge, X.: The impact of relative humidity on aerosol composition and evolution processes during wintertime in Beijing, China, *Atmos. Environ.*, 77, 927-934, <http://dx.doi.org/10.1016/j.atmosenv.2013.06.019>, 2013.
- 5 Sun, Y. L., Zhuang, G. S., Tang, A. H., Wang, Y., and An, Z. S.: Chemical characteristics of PM_{2.5} and PM₁₀ in haze-fog episodes in Beijing, *Environ. Sci. Technol.*, 40, 3148-3155, <https://doi.org/10.1021/es051533g>, 2006.
- Sun, Y. L., Jiang, Q., Wang, Z. F., Fu, P. Q., Li, J., Yang, T., and Yin, Y.: Investigation of the sources and evolution processes of severe haze pollution in Beijing in January 2013, *J. Geophys. Res. Atmos.*, 119, 4380-4398, <https://doi.org/10.1002/2014JD021641>, 2014.
- 10 Sun, Y. L., Jiang, Q., Wang, Z. F., Fu, P. Q., Li, J., Yang, T., and Yin, Y.: Investigation of the sources and evolution processes of severe haze pollution in Beijing in January 2013, *J. Geophys. Res. Atmos.*, 119, 4380-4398, <https://doi.org/10.1002/2014JD021641>, 2014.
- 15 Tan, J. H., Duan, J. C., Zhen, N. J., He, K. B., and Hao, J. M.: Chemical characteristics and source of size-fractionated atmospheric particle in haze episode in Beijing, *Atmos. Res.*, 167, 24-33, <http://dx.doi.org/10.1016/j.atmosres.2015.06.015>, 2016.
- Vereecken, L., Harder, H., and Novelli, A.: The reaction of Criegee intermediates with NO, RO₂, and SO₂, and their fate in the atmosphere, *Phys. Chem. Chem. Phys.*, 14, 14682, <https://doi.org/10.1039/c2cp42300f>, 2012.
- 20 Wang, G. H., Zhang, R. Y., Gomez, M. E., Yang, L. X., Zamora, M. L., Hu, M., Lin, Y., Peng, J. F., Guo, S., Meng, J. J., Li, J. J., Cheng, C. L., Hu, T. F., Ren, Y. Q., Wang, Y. S., Gao, J., Cao, J. J., An, Z. S., Zhou, W. J., Li, G. H., Wang, J. Y., Tian, P. F., Marrero-Ortiz, W., Secret, J., Du, Z. F., Zheng, J., Shang, D. J., Zeng, L. M., Shao, M., Wang, W. G., Huang, Y., Wang, Y., Zhu, Y. J., Li, Y. X., Hu, J. X., Pan, B., Cai, L., Cheng, Y. T., Ji, Y. M., Zhang, F., Rosenfeld, D., Liss, P. S., Duce, R. A., Kolb, C. E., and Molina, M. J.: Persistent sulfate formation from London Fog to Chinese haze, *Proc. Natl. Acad. Sci. U.S.A.*, 113, 13630-13635, <https://doi.org/10.1073/pnas.1616540113>, 2016.
- 25 Wang, Y., Zhuang, G., Tang, A., Yuan, H., Sun, Y., Chen, S., and Zheng, A.: The ion chemistry and the source of PM_{2.5} aerosol in Beijing, *Atmos. Environ.*, 39, 3771-3784, <https://doi.org/10.1016/j.atmosenv.2005.03.013>, 2005.
- Wang, Y., Zhang, Q., Jiang, J., Zhou, W., Wang, B., He, K., Duan, F., Zhang, Q., Philip, S., and Xie, Y.: Enhanced sulfate formation during China's severe winter haze episode in January 2013 missing from current models, *J. Geophys. Res. Atmos.*, 119, 4425-4440, <https://doi.org/10.1002/2013JD021426>, 2014a.
- 30 Wang, Y. S., Yao, L., Wang, L. L., Liu, Z. R., Ji, D. S., Tang, G. Q., Zhang, J. K., Sun, Y., Hu, B., and Xin, J. Y.: Mechanism for the formation of the January 2013 heavy haze pollution episode over central and eastern China, *Sci. China Earth Sci.*, 57, 14-25, <https://doi.org/10.1007/s11430-013-4773-4>, 2014b.



- Warneck, P.: The oxidation of sulfur(IV) by reaction with iron(III): a critical review and data analysis, *Phys. Chem. Chem. Phys.*, 20, 4020-4037, <https://doi.org/10.1039/c7cp07584g>, 2018.
- Xie, Y., Ding, A., Nie, W., Mao, H., Qi, X., Huang, X., Xu, Z., Kerminen, V. M., Petäjä T., and Chi, X.: Enhanced sulfate formation by nitrogen dioxide: Implications from in-situ observations at the SORPES Station, *J. Geophys. Res. Atmos.*, 120, 12679-12694, <https://doi.org/10.1002/2015JD023607>, 2015.
- Xu, F., Qiu, X., Hu, X., Shang, Y., Pardo, M., Fang, Y., Wang, J., Rudich, Y., and Zhu, T.: Effects on IL-1 β signaling activation induced by water and organic extracts of fine particulate matter (PM_{2.5}) in vitro, *Environ. Pollut.*, 237, 592-600, <https://doi.org/10.1016/j.envpol.2018.02.086>, 2018.
- Xu, L., Duan, F., He, K., Ma, Y., Zhu, L., Zheng, Y., Huang, T., Kimoto, T., Ma, T., Li, H., Ye, S., Yang, S., Sun, Z., and Xu, B.: Characteristics of the secondary water-soluble ions in a typical autumn haze in Beijing, *Environ. Pollut.*, 227, 296-305, <http://dx.doi.org/10.1016/j.envpol.2017.04.076>, 2017.
- Yang, Y. R., Liu, X. G., Qu, Y., An, J. L., Jiang, R., Zhang, Y. H., Sun, Y. L., Wu, Z. J., Zhang, F., Xu, W. Q., and Ma, Q. X.: Characteristics and formation mechanism of continuous hazes in China: a case study during the autumn of 2014 in the North China Plain, *Atmos. Chem. Phys.*, 15, 8165-8178, <https://doi.org/10.5194/acp-15-8165-2015>, 2015.
- Ye, C., Liu, P., Ma, Z., Xue, C., Zhang, C., Zhang, Y., Liu, J., Liu, C., Sun, X., and Mu, Y.: High H₂O₂ concentrations observed during haze periods in wintertime of Beijing: Importance of H₂O₂-oxidation in sulfate formation, *Environ. Sci. Technol. Lett.*, <https://doi.org/10.1021/acs.estlett.8b00579>, 2018.
- Yu, T., Zhao, D., Song, X., and Zhu, T.: NO₂-initiated multiphase oxidation of SO₂ by O₂ on CaCO₃ particles, *Atmos. Chem. Phys.*, 18, 6679-6689, <https://doi.org/10.5194/acp-18-6679-2018>, 2018.
- Zhang, Q., Quan, J. N., Tie, X. X., Li, X., Liu, Q., Gao, Y., and Zhao, D. L.: Effects of meteorology and secondary particle formation on visibility during heavy haze events in Beijing, China, *Sci. Total. Environ.*, 502, 578-584, DOI 10.1016/j.scitotenv.2014.09.079, 2015a.
- Zhang, R., Jing, J., Tao, J., Hsu, S. C., Wang, G., Cao, J., Lee, C. S. L., Zhu, L., Chen, Z., Zhao, Y., and Shen, Z.: Chemical characterization and source apportionment of PM_{2.5} in Beijing: Seasonal perspective, *Atmos. Chem. Phys.*, 13, 7053-7074, <https://doi.org/10.5194/acp-13-7053-2013>, 2013.
- Zhang, R., Sun, X. S., Shi, A. J., Huang, Y. H., Yan, J., Nie, T., Yan, X., and Li, X.: Secondary inorganic aerosols formation during haze episodes at an urban site in Beijing, China, *Atmos. Environ.*, 177, 275-282, <https://doi.org/10.1016/j.atmosenv.2017.12.031>, 2018.
- Zhang, X. Y., Gong, S. L., Shen, Z. X., Mei, F. M., Xi, X. X., Liu, L. C., Zhou, Z. J., Wang, D., Wang, Y. Q., and Cheng, Y.: Characterization of soil dust aerosol in China and its transport and distribution during 2001 ACE-Asia: 1. Network observations, *J. Geophys. Res.*, 108, <https://doi.org/10.1029/2002jd002632>, 2003.
- Zhang, Y. L., Huang, R. J., El Haddad, I., Ho, K. F., Cao, J. J., Han, Y., Zotter, P., Bozzetti, C., Daellenbach, K. R., Canonaco, F., Slowik, J. G., Salazar, G., Schwikowski, M., Schnelle-Kreis, J., Abbaszade, G., Zimmermann, R., Baltensperger, U., Prevot,



- A. S. H., and Szidat, S.: Fossil vs. non-fossil sources of fine carbonaceous aerosols in four Chinese cities during the extreme winter haze episode of 2013, *Atmos. Chem. Phys.*, 15, 1299-1312, <https://doi.org/10.5194/acp-15-1299-2015>, 2015b.
- Zhao, D., Song, X., Zhu, T., Zhang, Z., Liu, Y., and Shang, J.: Multiphase oxidation of SO₂ by NO₂ on CaCO₃ particles, *Atmos. Chem. Phys.*, 18, 2481-2493, <https://doi.org/10.5194/acp-18-2481-2018>, 2018.
- 5 Zheng, B., Zhang, Q., Zhang, Y., He, K. B., Wang, K., Zheng, G. J., Duan, F. K., Ma, Y. L., and Kimoto, T.: Heterogeneous chemistry: a mechanism missing in current models to explain secondary inorganic aerosol formation during the January 2013 haze episode in North China, *Atmos. Chem. Phys.*, 15, 2031-2049, <https://doi.org/10.5194/acp-15-2031-2015>, 2015a.
- Zheng, G. J., Duan, F. K., Su, H., Ma, Y. L., Cheng, Y., Zheng, B., Zhang, Q., Huang, T., Kimoto, T., Chang, D., Poschl, U., Cheng, Y. F., and He, K. B.: Exploring the severe winter haze in Beijing: the impact of synoptic weather, regional transport and heterogeneous reactions, *Atmos. Chem. Phys.*, 15, 2969-2983, <https://doi.org/10.5194/acp-15-2969-2015>, 2015b.
- 10 Zheng, M., Salmon, L. G., Schauer, J. J., Zeng, L. M., Kiang, C. S., Zhang, Y. H., and Cass, G. R.: Seasonal trends in PM_{2.5} source contributions in Beijing, China, *Atmos. Environ.*, 39, 3967-3976, <https://doi.org/10.1016/j.atmosenv.2005.03.036>, 2005.
- Zhu, T., Shang, J., and Zhao, D. F.: The roles of heterogeneous chemical processes in the formation of an air pollution complex and gray haze, *Sci. China Chem.*, 54, 145-153, <https://doi.org/10.1007/s11426-010-4181-y>, 2011.
- 15 Zhuang, G. S., Guo, J. H., Yuan, H., and Zhao, C. Y.: The compositions, sources, and size distribution of the dust storm from China in spring of 2000 and its impact on the global environment, *Chinese. Sci. Bull.*, 46, 895-901, <https://doi.org/10.1007/BF02900460>, 2001.



Figures and Tables

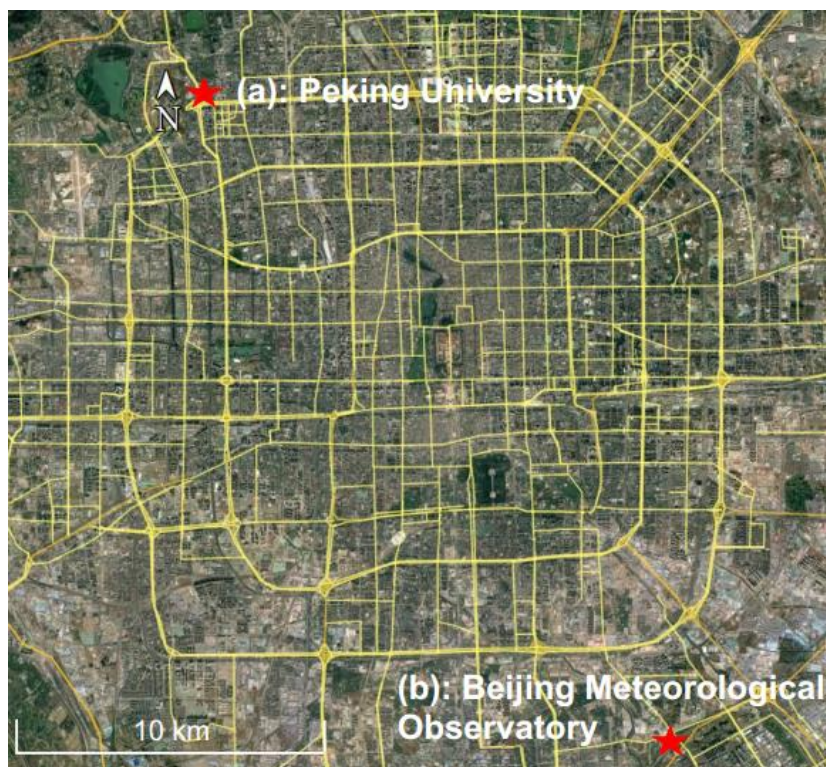


Figure 1. Sample sites in this study (red stars): (a) Peking University and (b) Beijing Meteorological Observatory.

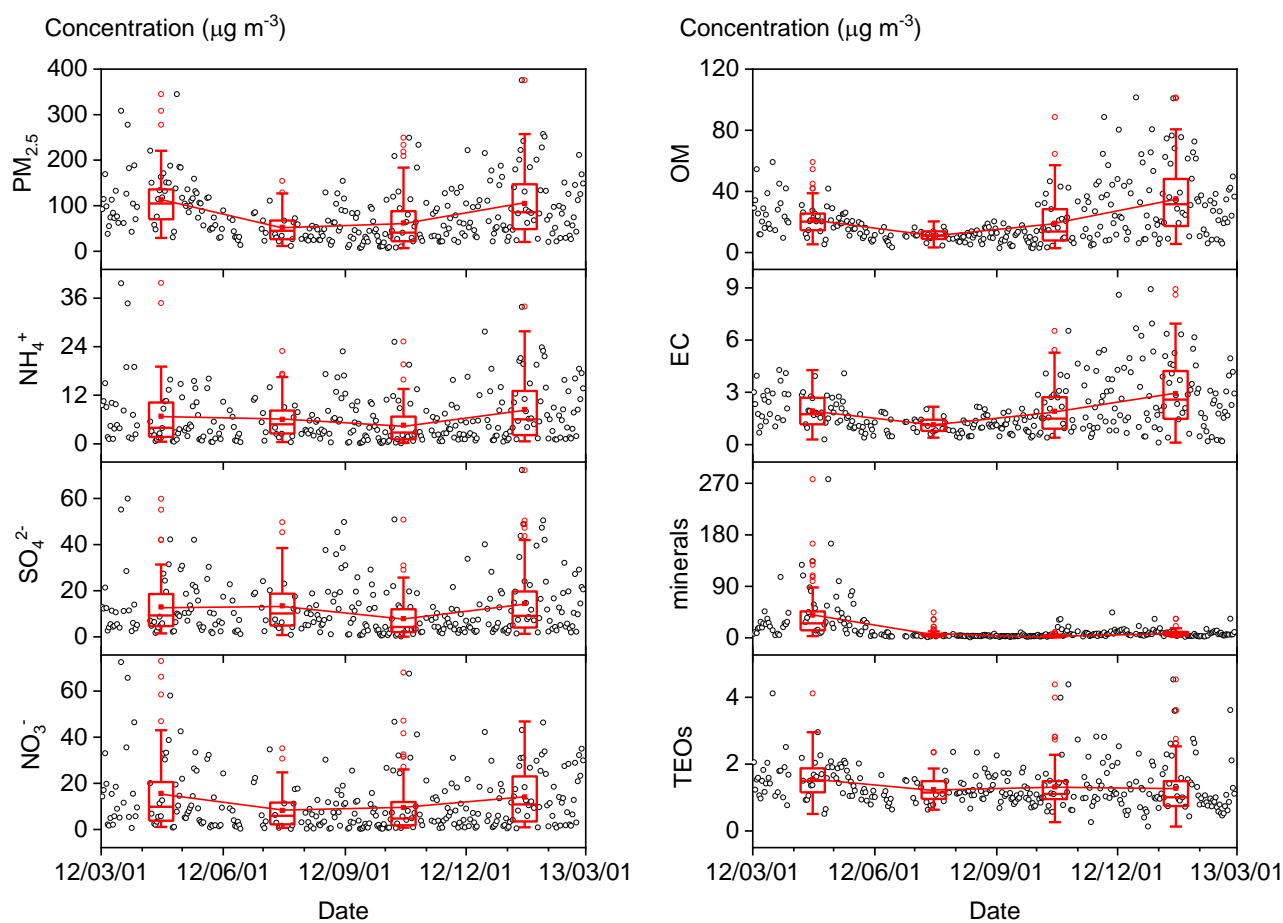


Figure 2. Time series of fine particulate matter ($PM_{2.5}$) concentrations and its seven major components from March 1 2012 to February 28 2013 (open black circles). The boxes represent, from top to bottom, the 75th, 50th, and 25th percentiles for each season. The whiskers, solid red squares, and open red circles represent 1.5 times the interquartile range (IQR), seasonal mean values, and outlier data points, respectively.

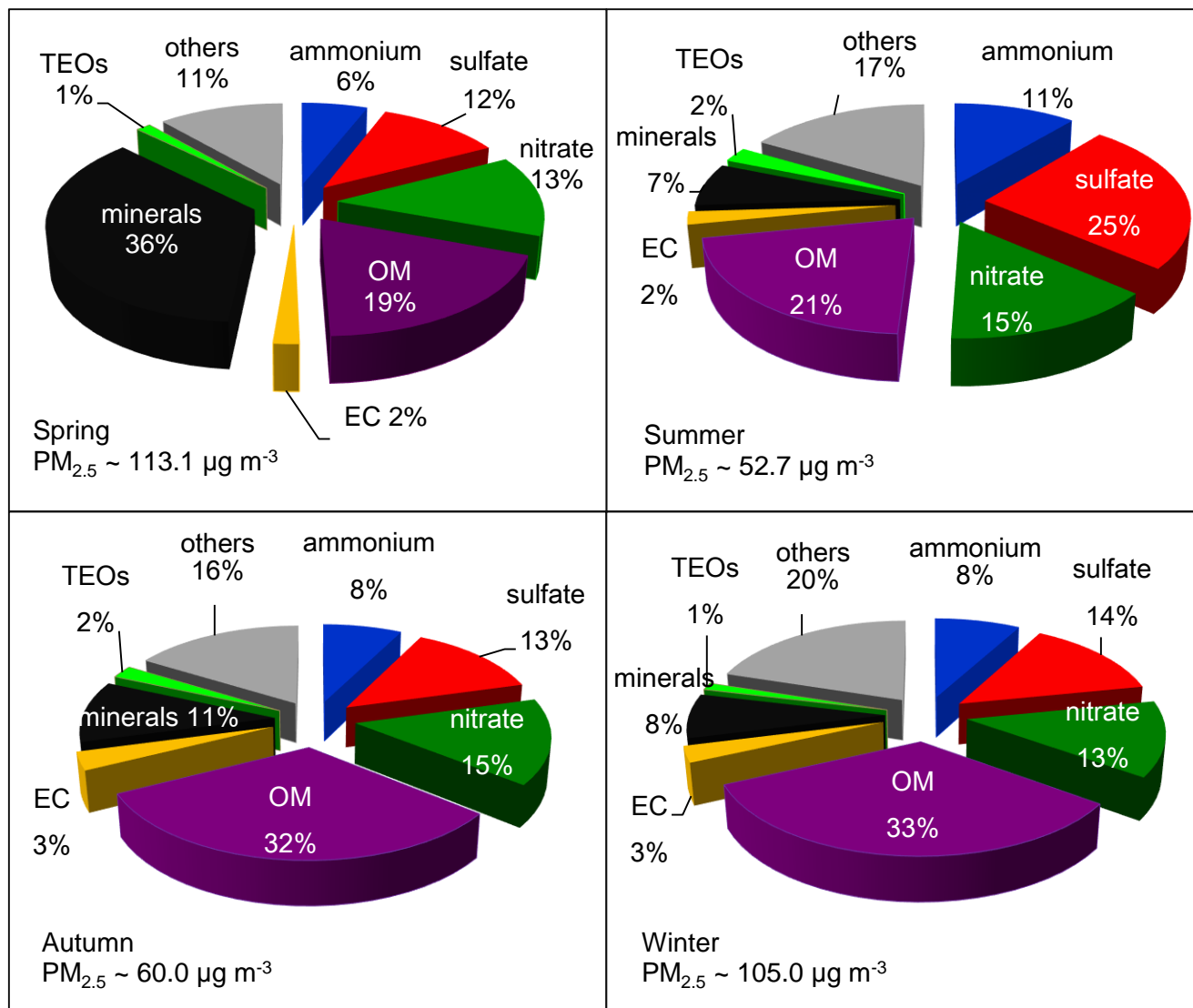


Figure 3. Seasonal variations in PM_{2.5} and its seven major components from March 1 2012 to February 28 2013.

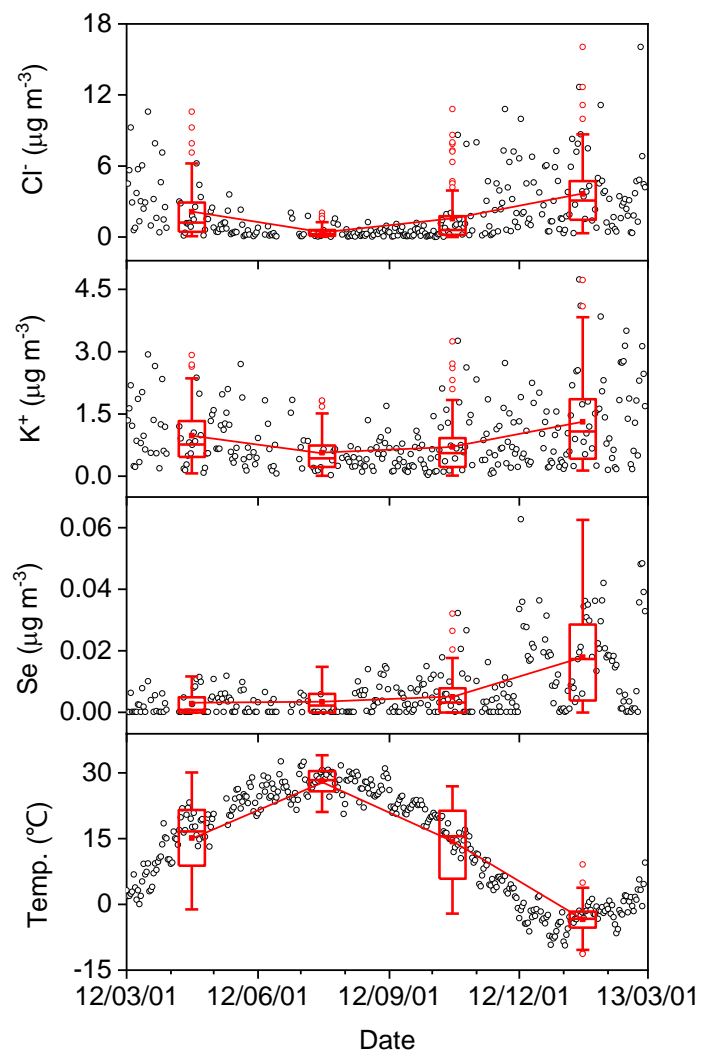


Figure 4. Time series of Cl^- , K^+ , Se, and temperature from March 1 2012 to February 28 2013 (open black circles). The boxes represent, from top to bottom, the 75th, 50th, and 25th percentiles for each season. The whiskers, solid red squares, and open red circles represent 1.5 times the IQR, seasonal mean values, and outlier data points, respectively.

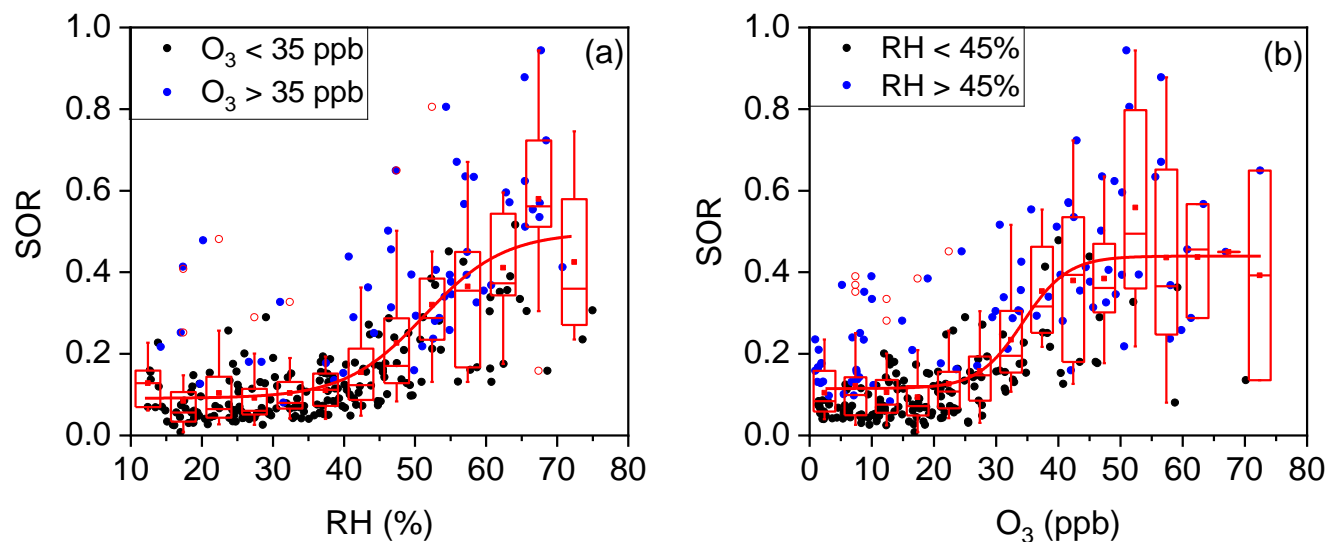


Figure 5. (a) Plot of the sulfur oxidation ratio (SOR) against relative humidity (RH) grouped by O_3 concentration. The solid blue circles represent $O_3 > 35$ ppb and the solid black circles represent $O_3 < 35$ ppb. (b) Plot of the SOR against O_3 grouped by RH. The solid blue circles represent $RH > 45\%$ and the solid black circles represent $RH < 45\%$. The boxes represent, from top to bottom, the 75th, 50th, and 25th percentiles in each bin ($\Delta RH = 5\%$; $\Delta O_3 = 5$ ppb). The whiskers, solid red squares, and open red circles represent 1.5 times the IQR, seasonal mean values, and outlier data points, respectively. The red lines are best fits to mean values based on a sigmoid function (dose-response). Data for days with rain or snow were excluded from these plots.

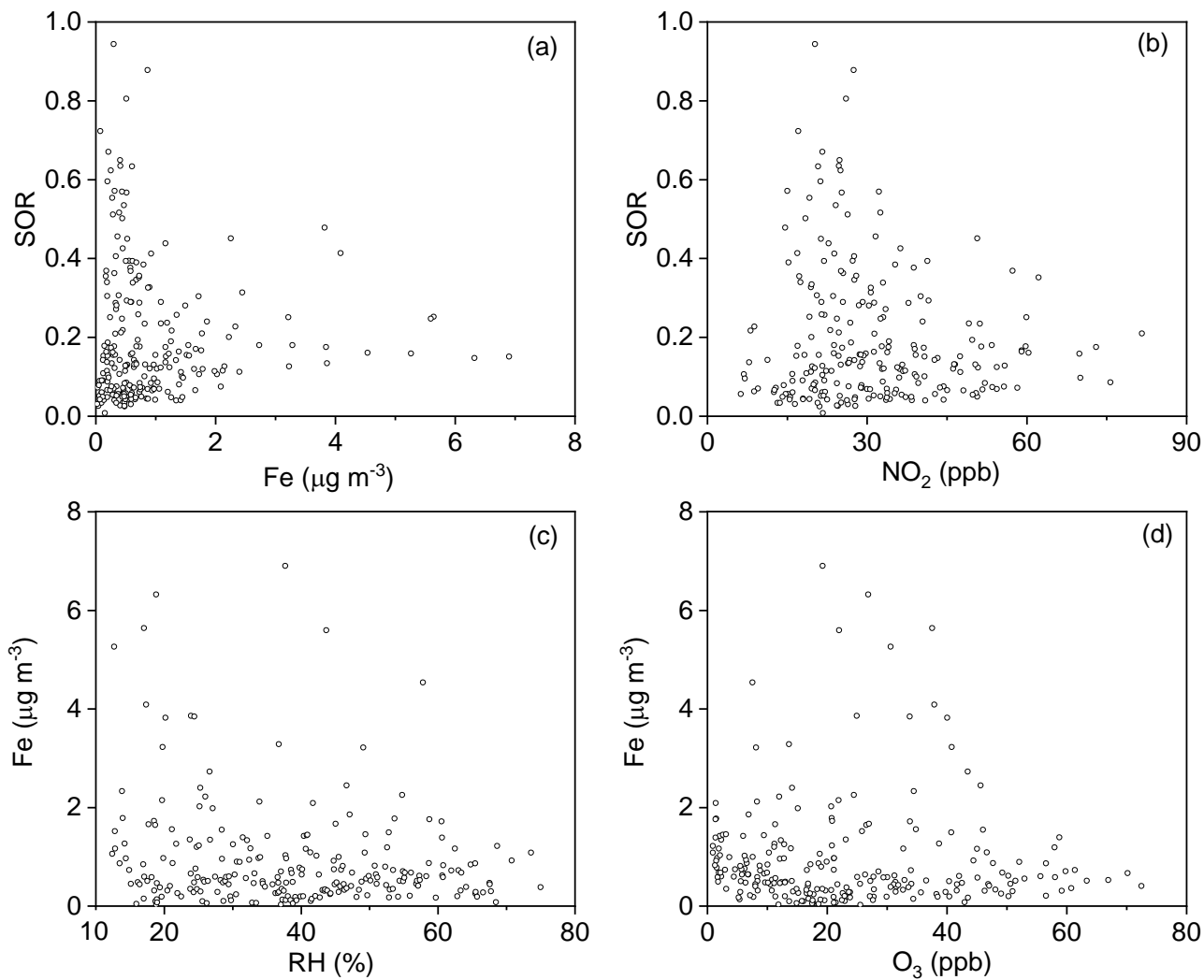


Figure 6. Plots of SORs against (a) Fe and (b) NO₂. Plots of Fe against (c) RH and (d) O₃. Data for days with rain or snow were excluded from these plots.

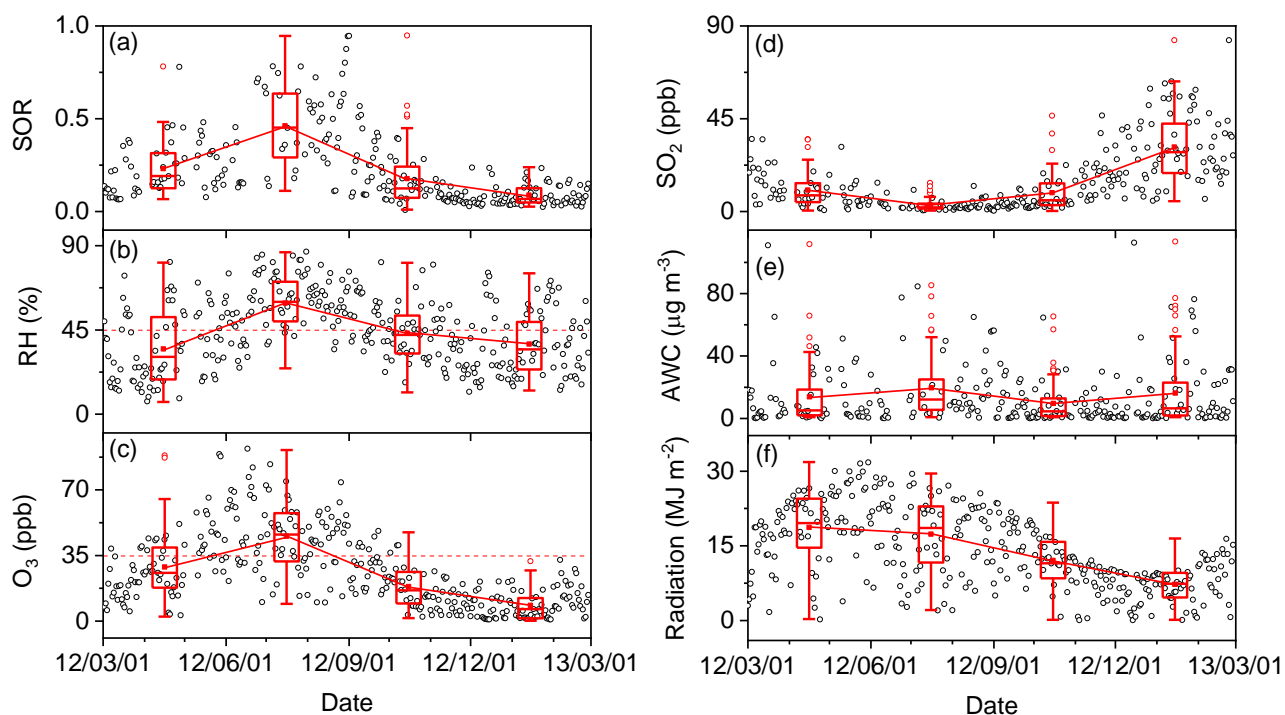


Figure 7. Time series of (a) SORs, (b) RH, (c) O₃, (d) SO₂, (e) aerosol water content (AWC), and (f) solar radiation from March 1 2012 to February 28 2013 (open black circles). The boxes represent, from top to bottom, the 75th, 50th, and 25th percentiles for each season. The whiskers, solid red squares, and open red circles represent 1.5 times the IQR, seasonal mean values, and outlier data points, respectively. The horizontal dashed lines in panels (b) and (c) represent thresholds of RH = 45% and O₃ = 35 ppb, respectively.

5

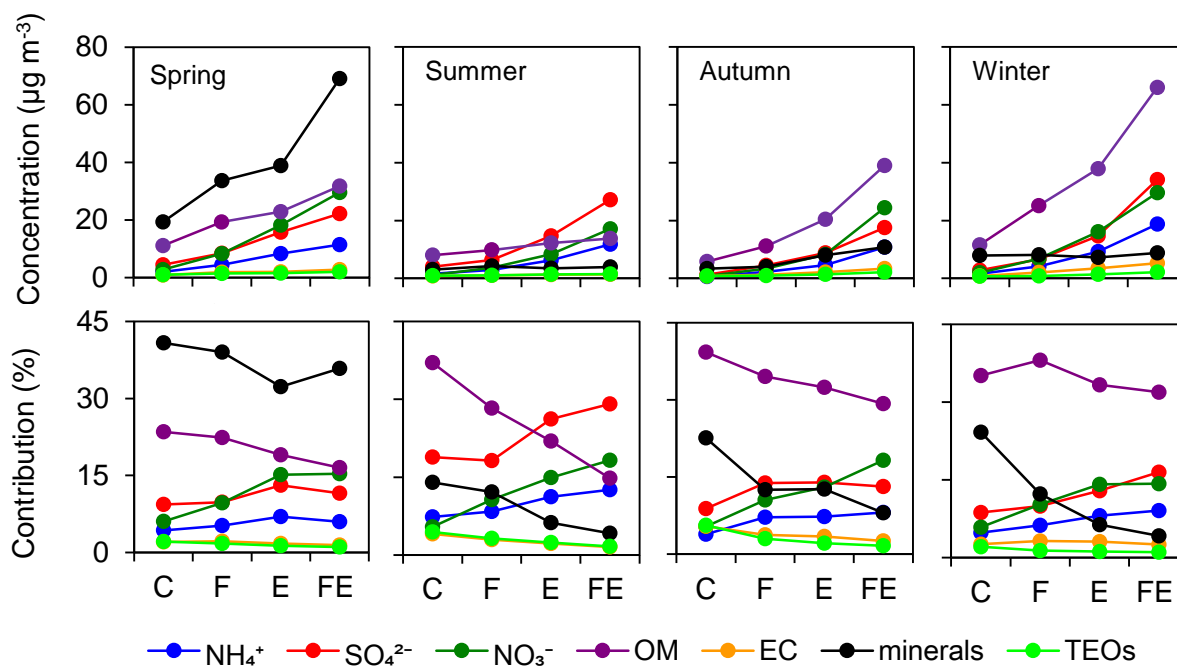


Figure 8. Variations in the mean concentrations (upper panels) and contributions (lower panels) of the seven major components of PM_{2.5} with pollution levels in each season. C, clean; F, formation; E, evolution; FE, further evolution.

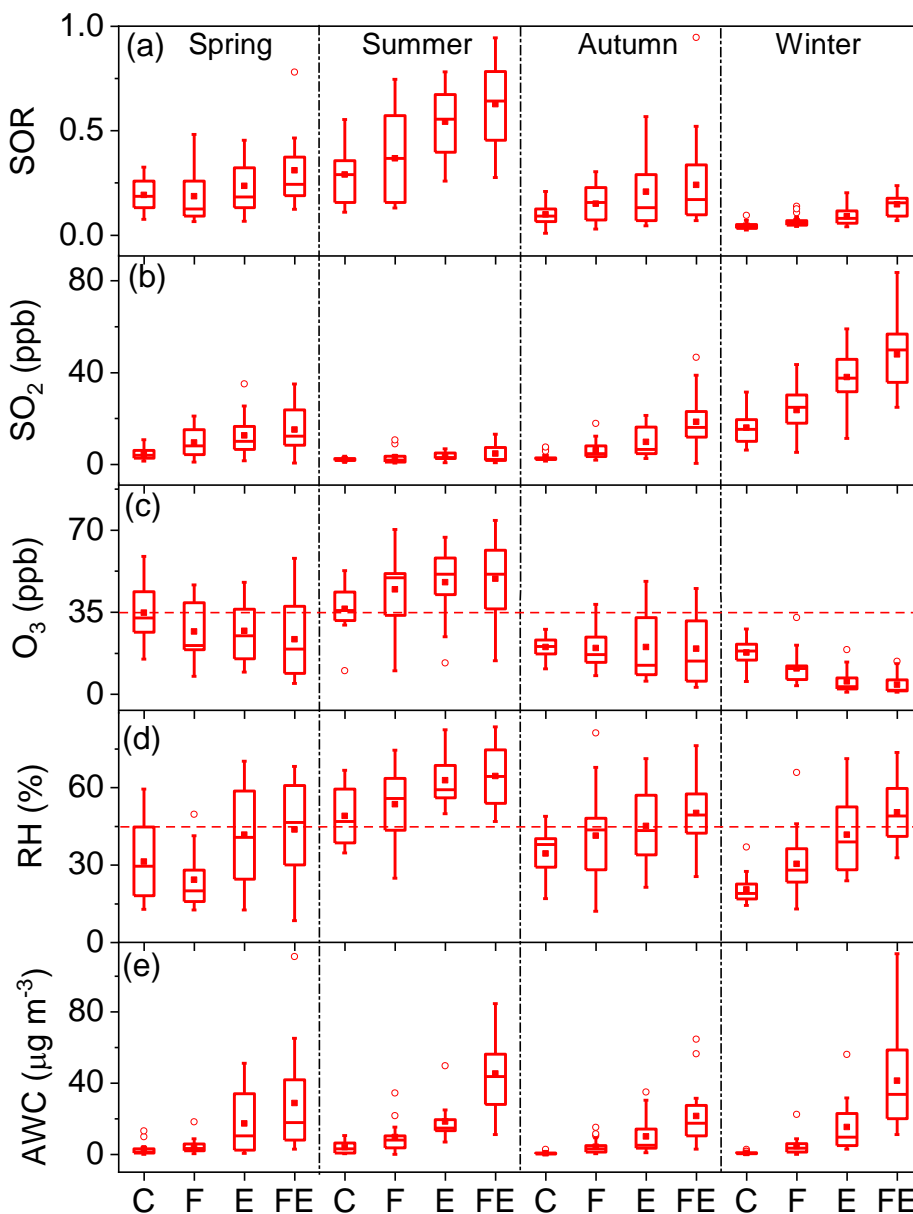


Figure 9. Variations in (a) SORs, (b) SO₂, (c) O₃, (d) RH, and (e) AWC with pollution levels in each season. C, clean; F, formation; E, evolution; FE, further evolution. The boxes represent, from top to bottom, the 75th, 50th, and 25th percentiles for each pollution level. The whiskers, solid red squares, and open red circles represent 1.5 times the IQR, seasonal mean values, and outlier data points, respectively. The horizontal dashed lines in panels (c) and (d) represent thresholds of O₃ = 35 ppb and RH = 45%, respectively.

**Table 1.** Annual and seasonal mean concentrations ($\mu\text{g m}^{-3}$, ± 1 standard deviation) of $\text{PM}_{2.5}$ and its seven major components.

| Component | Annual | Spring | Summer | Autumn | Winter |
|--------------------------------------|-----------------|------------------|-----------------|-----------------|------------------|
| $\text{PM}_{2.5}$ | 84.1 ± 63.1 | 113.1 ± 62.0 | 52.7 ± 32.6 | 60.0 ± 51.3 | 105.0 ± 71.7 |
| NH_4^+ | 6.4 ± 6.4 | 6.7 ± 7.3 | 5.9 ± 5.0 | 4.5 ± 4.8 | 8.4 ± 7.4 |
| SO_4^{2-} | 12.0 ± 12.2 | 12.9 ± 12.4 | 13.3 ± 11.5 | 7.9 ± 8.7 | 14.5 ± 14.4 |
| NO_3^- | 11.5 ± 12.6 | 15.0 ± 16.0 | 7.6 ± 8.0 | 9.0 ± 11.8 | 13.6 ± 12.1 |
| OM | 22.7 ± 18.1 | 21.5 ± 10.5 | 11.1 ± 3.8 | 19.2 ± 16.1 | 35.2 ± 23.4 |
| minerals | 14.7 ± 27.0 | 40.7 ± 45.0 | 3.7 ± 1.6 | 6.5 ± 7.0 | 8.0 ± 5.6 |
| TEOs | 1.3 ± 0.7 | 1.5 ± 0.6 | 1.2 ± 0.4 | 1.3 ± 0.7 | 1.3 ± 0.8 |
| EC | 2.1 ± 1.5 | 1.9 ± 1.0 | 1.1 ± 0.5 | 1.9 ± 1.3 | 2.9 ± 2.0 |